Initial Thickness Measurements and Insights into Crystal Growth of Methane Hydrate Film

Sheng-Li Li, Chang-Yu Sun, Bei Liu, Xiu-Jun Feng, and Feng-Guang Li
State Key Laboratory of Heavy Oil Processing, China University of Petroleum, Beijing 102249, China

Li-Tao Chen
Steacie Institute for Molecular Sciences, National Research Council of Canada, Ottawa, Ontario, Canada K1A 0R6

Guang-Jin Chen
State Key Laboratory of Heavy Oil Processing, China University of Petroleum, Beijing 102249, China

DOI 10.1002/aic.13987
Published online January 14, 2013 in Wiley Online Library (wileyonlinelibrary.com)

The initial thickness of methane hydrate film was directly measured by suspending a single methane bubble in water at 274.0, 276.0, and 278.0 K. The results show that the initial hydrate film thickness decreases from tens of micrometers to about 10 μm with the subcooling increased from 0.5 K to about 3 K. When subcooling is higher than 1.0 K, all initial film thickness data measured under different temperatures vary inversely with the subcooling. Notable three-dimensional growths of hydrate crystals of different sizes and shapes at film front and emergence of new crystal were clearly observed at lower subcooling that resulting in the rougher surface of hydrate film and uncertainty of initial thickness measurement under lower subcooling. The hydrate film growth was dominated by film growth in thickness, not by lateral growth at low subcooling. The growth in thickness of hydrate shell covering one whole bubble surface was also investigated. © 2013 American Institute of Chemical Engineers *AIChE J*, 59: 2145–2154, 2013
Keywords: methane hydrate, film thickness, three-dimensional, crystal growth

Introduction

Natural gas hydrate is a kind of large alternative energy resource with huge reserves.[1] Gas hydrate can also be applied to gas storage,[2–4] transportation,[5–7] and gas mixture separation.[8] The growth kinetic law of gas hydrate is the basis of further studies on the accumulation of *in situ* natural gas hydrate[9] and the developments of hydrate-based applied technologies.[10] In general, gas hydrate growth initiates at water/guest-fluid interface. Once one stable hydrate crystal forms at water/guest-fluid interface, it grows not only laterally along the interface but also in the direction vertical to the interface, thereby grows to a hydrate film of certain thickness between water and guest fluid.[11,12]

The lateral growth of hydrate film at the gas/liquid or gas/solid interface has been experimentally and/or theoretically studied by several groups.[11,13–18] Arguments regarding the control steps of lateral growth of hydrate film are mainly on intrinsic kinetics and heat transfer. The advantage of heat-transfer control models is that the film thickness could be formulated into the film growth kinetic equation.[14,15,18] In this way, it is possible to establish the relationship between lateral growth rate and the bulk hydrate-phase growth rate. On the basis of the heat-transfer model developed by Mori,[14] Peng et al.[18] presented a more precise model of lateral growth of hydrate film by introducing an assumption that the initial thickness of hydrate film varies with driving force inversely. Here, the initial thickness refers to the front thickness of hydrate film growing laterally and should not be confused with the final grown thickness of hydrate films, which mainly depends on the mass transfer in the direction normal to the film.[14] Because the driving force for mass transfer of guest components or water through hydrate film increases with the increasing subcooling, the thickening rate of hydrate film might increase with it too. Thus, the final thickness of hydrate film might increase with the increasing subcooling.[19] It is important to establish the relationship between the initial film thickness and subcooling in modeling hydrate lateral growth rate.[18–21] The initial thickness is also crucial for investigating the vertical growth of hydrate film. However, the experimental data directly manifesting the influence of subcooling upon the initial thickness of hydrate film are scarcely reported, because they are hard to measure. Previous reports related to thickness of hydrate film mainly focused on the measurements[19,22] of growth rate in hydrate film thickness and final film thickness with respect to different subcoolings. There also exist some measurements in the literature about the thickening of hydrate film in the vertical direction after initial lateral growth.[21,23–27] However, the initial thickness of hydrate film was not given definitely. Ohmura et al.[21] measured CH_2FCF_3 hydrate film thickness using laser interferometry and found that the film thickness

Correspondence concerning this article should be addressed to C.-Y. Sun at cysun@cup.edu.cn or G.-J. Chen at gjchen@cup.edu.cn.

at the beginning time increases with the decrease of the subcooling. But in their experiments, the first data points are several tens of minutes after film formation because of the time required for adjusting their optical system and the film thickness obtained is not an actual initial film thickness as the authors pointed out. Peng et al.[18] only qualitatively proved that there exists inverse relation between the initial thickness and the subcooling by observing the transparency of the hydrate film. Thus, more precise measurement on initial film thickness is required to establish the relationship between initial thickness and subcooling quantitatively.

The location of the initial hydrate film front is another important basic information for modeling the lateral growth of hydrate film at the water-/guest-phase interface. Because there is no direct experimental information on it, there exist several assumptions about the location of hydrate film front. In his convective heat-transfer model, Mori[14] assumed that half of the film front is in the water phase and the other half is in the guest phase, whereas Mochizuki and Mori[15] assumed that the entire front is in the water phase. Peng et al.[18] proposed a more flexible assumption that a part of thickness x of hydrate film front is in the guest phase and another part of thickness $\delta - x$ is in the water phase. The value of x was thought to be guest composition dependent. However, they did not give the method to determine the value of x. Therefore, delicate experimental investigation should be carried out to clarify the location of hydrate film front.

Study on the growth mechanism of hydrate crystals is also of great importance for modeling of macroscopic kinetics of hydrate formation with respect to different application fields of gas hydrate. Many theoretical and experimental studies[23,28–31] about the hydrate crystal growth have been performed with respect to different subcoolings and compositions of gas mixtures. However, a further understanding of the growth patterns of hydrate crystals is necessary, in view that most of those investigations only examined the formation pattern of hydrate crystals in two dimension. As already reviewed,[29,31–33] the studies of *in situ* observations of hydrate crystals in three dimensions were only performed on structure II[29,31] and structure H[32] hydrates formed with two guests together. So far, to our knowledge, the crystal growth in three dimension of a simple structure I or structure II hydrate formed with only one guest component has not been investigated.

In this work, the location of hydrate film front was determined, and the initial thickness of methane hydrate film on the surface of bubble suspended in water was measured directly by a microscope for the first time. The relationship between the initial film thickness and subcooling was further investigated. The process of methane hydrate crystals growth on the surface of bubble was also observed using the microscope, and the three-dimensional (3-D) growth patterns of the hydrate crystals were discussed. Additionally, the growth of hydrate shell covering the surface of bubble in thickness was observed.

Experimental

Equipment and materials

The schematic diagram of the experimental device is shown in Figure 1. The main part of the apparatus is a high-pressure cell with an inner space of 36 mm in diameter and 15 mm in axial length. There are a pair of glass windows installed in two opposite sides of the cell, through which the phenomenon occurred in the cell can be observed using a microscope and recorded by a CCD camera conveniently. A needle with a diameter of 2.996 mm is extended into the cell from the bottom, through which gas can be injected into the cell to produce gas bubble. The pressure of the cell is controlled by supplying methane from a gas cylinder through a pressure regulating valve with a maximum scale of 20 MPa. The temperature inside the cell is controlled by an air bath, and the temperature can be adjusted in the range of 253.2–293.2 K. The system temperatures are detected by three Eurotherm temperature controllers with an average uncertainty of ± 0.1 K. All the pressure gauges are calibrated using a standard RUSKA deadweight pressure gauge with an uncertainty of $\pm 0.25\%$. Analytical grade CH_4 (99.99%) supplied by Beijing Beifen Gas Industry Corp. is used in the experiment. The water used in the experiments is distilled twice, and its conductivity is found to be less than 10^{-4} S m^{-1}.

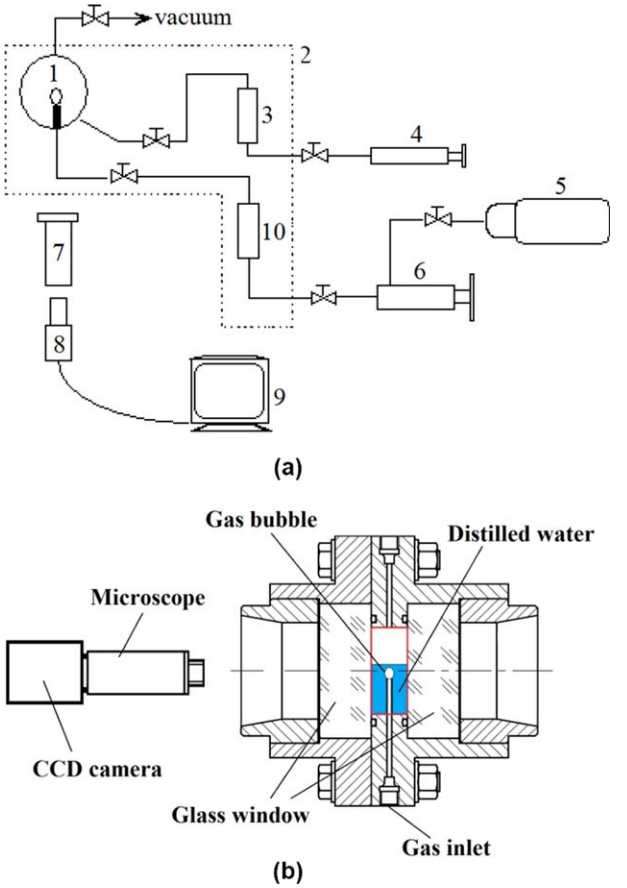

Figure 1. (a) Schematic diagram of the experimental apparatus: 1, test cell; 2, thermostat; 3, liquid sample cylinder; 4, JEFRI 10-1-12-NA pump; 5, gas cylinder; 6, JEFRI 100-1-10-HB pump; 7, microscope; 8, CCD camera; 9, computer; and 10, gas sample cylinder. (b) Schematic diagram of high-pressure cell.

[Color figure can be viewed in the online issue, which is available at wileyonlinelibrary.com.]

Experimental procedures

At first, the entire system is purged with gas and then evacuated. Subsequently, distilled water is charged into the

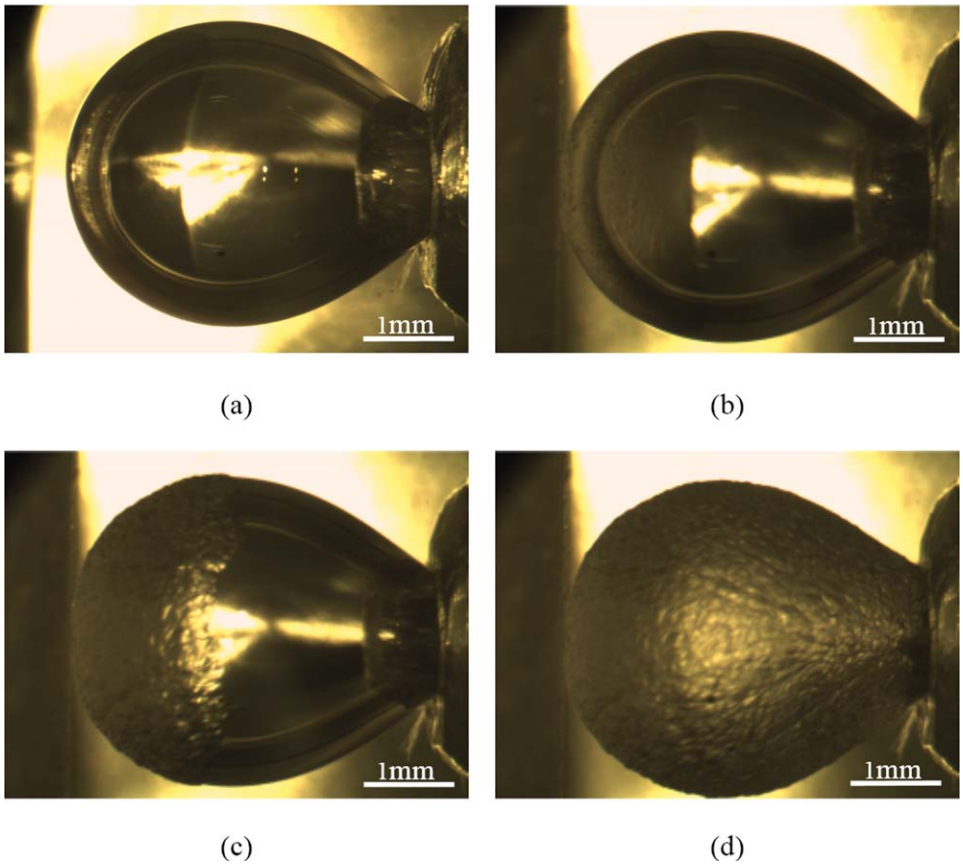

Figure 2. Pictures of methane hydrate film growth on the surface of a suspended bubble in water (rotated anticlockwise 90°).

(a) A methane gas bubble suspends in water before the formation of hydrate layer atop the water phase; (b) a hydrate layer forms at the bulk gas–water interface, and a bubble is injected slowly through the needle to contact with the hydrate layer. Once the bubble contacts with the hydrate layer, the hydrate film growth on the surface of the bubble starts; (c) the hydrate film is growing on the surface of the bubble; and (d) the suspended bubble is wholly covered with hydrate film. The hydrate film growth processes and crystal morphology changes in experiments can be repeated. [Color figure can be viewed in the online issue, which is available at wileyonlinelibrary.com.]

high-pressure cell until about three-fourths of its volume is filled. The system temperature is then adjusted to a desired value through the air bath. After the system temperature becomes stable, methane gas is introduced continuously into the cell through the needle at the bottom until the system pressure is significantly higher than the equilibrium pressure for hydrate formation. Subsequently, the gas is discharged slowly out of the cell from a valve on the top of the cell. After that, the high-pressure cell is recharged with methane gas to agitate water phase, and this process of gas charging and discharging is continued to reduce the induction time until a quantity of gas hydrate forms atop the water phase. The gas–liquid equilibrium can also be easily established in region near gas–liquid interface through this process. The cell is depressurized to dissociate the hydrate thoroughly, while the temperature of the air bath keeps constant. Afterward, gas is injected into the cell and maintained at a desired pressure higher than the equilibrium value of hydrate formation at the specified temperature.

Following above preparing procedures, the hydrate film growth experiment is carried out as illustrated in Figure 2. At first, a methane hydrate layer is formed at the bulk gas/liquid interface in the cell (the left of Figures 2a,b). A methane gas bubble is then injected slowly into the cell through the needle. When the bubble just contacts to the hydrate layer, the hydrate film lateral growth on the suspended bubble starts and eventually terminates when the surface of suspended bubble is fully covered with hydrate film (Figures 2b–d). Afterward, system pressure is decreased to the atmospheric pressure to dissociate hydrate, and the gas and water are discharged out of the cell. The fresh distilled water is charged into the cell for another experimental run.

The whole methane hydrate film growth process is observed by using a microscope, recorded by a CCD camera, and stored by a computer. The image of a gas bubble recorded is quantified in an established coordinate system as shown in Figure 3. As shown in Figure 3b, there exists obvious distance between the outer surface of growing hydrate film and the surface of the gas bubble. Two parallel lines are drawn tangently to the outer surface of hydrate film and that of the gas bubble. The minimum distance between the two parallel lines is measured directly and taken as the thickness of hydrate film front, that is, the initial thickness of hydrate film.

Results and Discussion

Film front location and thickness

A series of experiments on the lateral growth of hydrate film on the surface of the methane bubble suspended in water were performed, and the initial film thicknesses were measured at three specified temperatures of 274.0, 276.0, and 278.0 K and different subcooling ΔT values with the

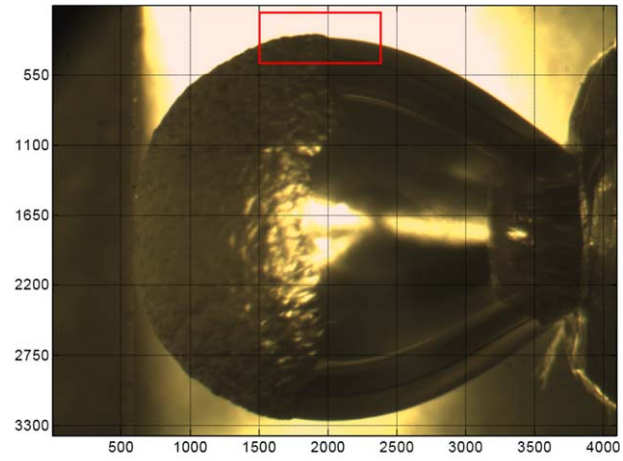

(a)

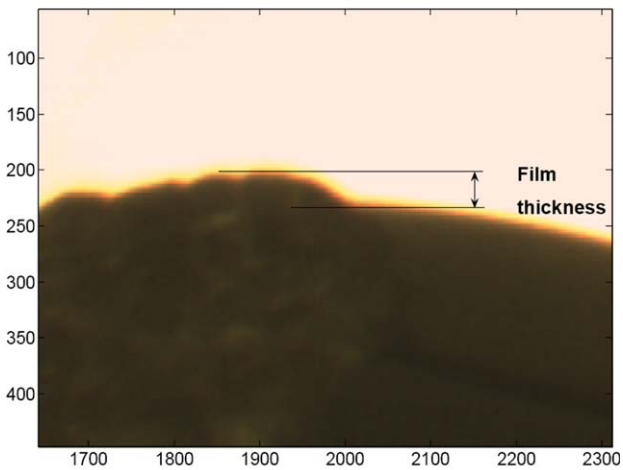

(b)

Figure 3. (a) A coordinate system established for the image of hydrate film growth on the suspended bubble and (b) the thickness measurement carried out in the coordinate.

The unit for length in (a) and (b) is micrometer. [Color figure can be viewed in the online issue, which is available at wileyonlinelibrary.com.]

method mentioned earlier. The ΔT is defined as $\Delta T = T^{eq} - T^{exp}$, where T^{exp} is the temperature for hydrate film growth specified in the experiment; T^{eq} is the equilibrium formation temperature of hydrate at experimental pressure, which is calculated with the Chen–Guo hydrate model.[34] The experimental results are shown in Figures 4 and 5 and Table 1.

Figure 4 shows the initial hydrate film formed on the surface of a bubble in three cases of different subcoolings and temperatures. It can be directly seen that the film front of methane hydrate is entirely in the water phase in all three cases. The observations of other researchers[25,28] also indicated that hydrate films first formed to intervene between the gas guest and liquid water and then grew toward the liquid water. The determination that whole film front is in water is also the basis on which the initial film thickness was measured in this work, because the vertical distance of the surface of hydrate film and that of the bubble was taken as the initial film thickness.

One can see from Table 1 that the initial film thickness decreases with the increase of ΔT when temperature is specified. To better display the influences of the subcooling and temperature upon the initial thickness of hydrate film, the measured initial film thickness data were plotted against $1/\Delta T$ in Figure 5. One can see that the initial film thickness mainly depends on the subcooling at higher subcooling region; its dependence on temperature is unremarkable. When the subcooling is higher than 1.0 K, all initial film thickness data measured under three different temperatures can be fitted with the following Eq. 1 satisfyingly as shown in Figure 5, with a correlation coefficient $R^2 = 0.91$. For comparison, the initial thickness data of hydrate film formed at the planar bulk methane/water interface measured by Taylor et al.[19] at a higher subcooling of 5.2 K were also plotted in Figure 5. One can see that their experimental data are also in good agreement with the fitted line by Eq. 1. These results demonstrate that Peng et al.'s[18] assumption that the initial thickness of hydrate film varies with the subcooling inversely is acceptable in higher subcooling region, that is, $\Delta T > 1.0$ K.

$$\delta = k/\Delta T \tag{1}$$

where δ is the initial thickness of hydrate film and k is the inverse proportional coefficient.

However, at very low subcoolings, the experimental data deviate from the fitted line obviously and become strongly temperature dependent. This phenomenon might be attributed to the fact that the growth of hydrate film is dominated by the film growth in thickness, but not by lateral growth. That will be discussed in more detail in the following section.

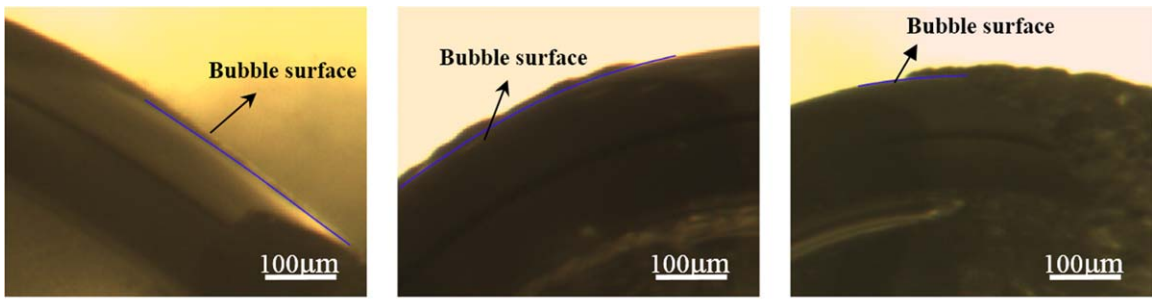

274.0 K, ΔT =2.0 K. 276.0 K, ΔT =0.9 K. 278.0 K, ΔT =0.7 K.

Figure 4. Initial hydrate film formed on the surface of a bubble in three cases with different subcoolings and temperatures.

[Color figure can be viewed in the online issue, which is available at wileyonlinelibrary.com.]

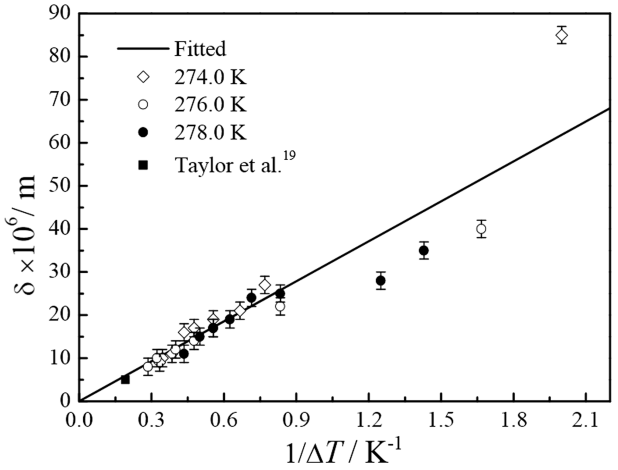

Figure 5. Variation of CH_4 hydrate initial film thickness with subcooling at different specified temperatures.

Using Peng et al.'s[18] kinetic model for lateral growth of hydrate film as well as the parameters determined by them, the initial thickness of hydrate film was calculated by assuming that whole film front was in water phase. The calculation results with respect to three temperatures specified in this work are tabulated in Table 2. Compared with the experimental data, the calculated initial thickness value is a little smaller at the same subcooling and temperature, although they are in the same magnitudes of order. This might be due to the following reasons. First, in the heat-transfer model,[14,18] the heat-transfer surface is simplified as a surface of semicircular whose area is smaller than that of the actual hydrate film front shaped as polyhedron. Second, the porous structure[35] of hydrate film is ignored, as the film is assumed to be solid and of uniform thickness, then the heat-transfer area is smaller than actual one. As a result, the efficiency of heat transfer in the experiment is higher than that modeled. Therefore, the calculated initial thickness is thinner than the actual ones. This comparison of calculated results with experimental data also demonstrates that the conclusion that the whole film front is in water phase is accurate. Otherwise, the calculated value of initial thickness of hydrate film would become further smaller. (If the film front is partly or entirely in the gas phase, parameter C in heat-transfer model[18] will be smaller, as the thermal conductivity of gas is much smaller than that of water. Therefore, when under a certain lateral growth rate υ_f and subcooling ΔT, a smaller initial film thickness is calculated by the equation $\upsilon_f \delta = C\ \Delta T^{3/2}$).[18]

Table 1. The Initial Film Thickness of Methane Hydrate Measured on the Surface of Bubble at Different ΔT and Three Different Specified Temperatures (the Hydrate Film Thicknesses Data Measured in the Experiments Are Reproducible Within the Standard Deviations)

T (K)	P (MPa)	ΔT (K)	$\delta \pm 2$ (μm)
274.0	2.91	0.5	85
	3.17	1.3	27
	3.23	1.5	21
	3.34	1.8	19
	3.44	2.1	17
	3.52	2.3	16
	3.63	2.6	11
	3.74	2.9	10
	3.78	3.0	9
276.0	3.63	0.6	40
	3.86	1.2	22
	4.12	1.8	17
	4.25	2.1	14
	4.43	2.5	12
	4.72	3.1	10
	4.93	3.5	8
278.0	4.53	0.7	35
	4.57	0.8	28
	4.77	1.2	25
	4.87	1.4	24
	4.98	1.6	19
	5.09	1.8	17
	5.20	2.0	15
	5.37	2.3	11

Table 2. The Initial Film Thicknesses δ and k Value in Eq. 1 Calculated at Different Temperatures with the Model of Peng et al.[18] by Assuming the Whole Film Front Is in Water Phase

T (K)	δ (μm)	$k \times 10^5$ (m K)	ΔT (K)
274.0	6.60–19.81	1.981	3.0–1.0
276.0	5.55–16.64	1.664	3.0–1.0
278.0	4.77–14.30	1.430	3.0–1.0

By considering the geometrical effect on heat transfer in hydrate-film front, Mochizuki and Mori[15] proposed a heat-transfer control model. Using this model, the initial thickness of methane hydrate film at a subcooling of about 10 K was estimated to be 10–20 μm, which is too thick to be acceptable compared with present experimental results. The reason might be that the heat-transfer rate was over estimated in their model. The initial film thickness of methane hydrate calculated by Freer et al.[17] based on a convective heat transfer plus intrinsic kinetics control mechanism ranges from 2 to 5 μm in a subcooling range of 2–11 K and a temperature range of 274.15–277.15 K. Their calculation results agree with our experimental data only at higher subcoolings. Overall, Peng et al.'s model gives the good evaluation on initial thickness of methane hydrate film. (During the building of convective heat-transfer control model in Peng et al.'s work, it was assumed that the thickness of hydrate films is inversely proportional to the subcooling. The relationship between the lateral film growth rate and the subcooling can be represented using the equation, that is, $\upsilon_f = \psi \Delta T^{5/2}$, for all the systems examined.)

Figure 6 shows the comparison of morphologies of methane hydrate films formed under different temperatures and different subcoolings. As can be seen, the morphology of hydrate film mainly depends on the subcooling. The surface of hydrate film formed at higher subcooling is smoother than that formed at lower subcooling. The roughness of the surface of hydrate film formed at $\Delta T < 1.0$ K is quite noticeable, whereas the hydrate film formed at $\Delta T > 2.0$ K is quite smooth. The difference in the roughness of hydrate film surface may be ascribed to the nonuniform growths of single crystals in film front accompanying with the lateral growth of hydrate film, which is also strongly subcooling dependent and will be discussed in following section in detail.

The 3-D growth pattern of CH_4 hydrate

With the measurements of initial film thickness, the crystal growth in three dimension of CH_4 hydrate was also observed

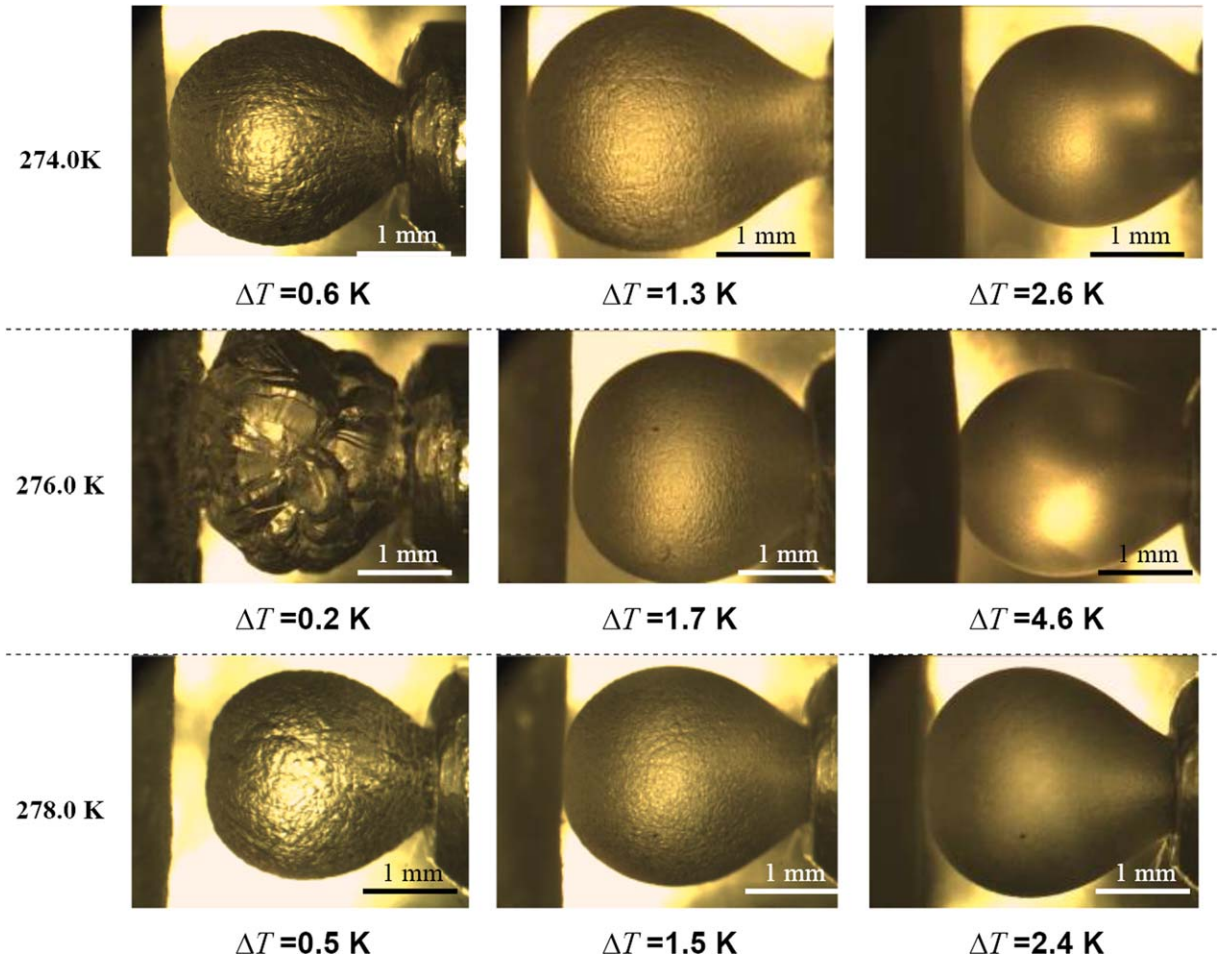

Figure 6. Variation of CH_4 hydrate shells covered on the surface of bubble with the subcooling at different specified temperatures.

[Color figure can be viewed in the online issue, which is available at wileyonlinelibrary.com.]

under different experimental conditions. The polygonal shapes of the single crystals[36] as well as their variation with elapsed time were observed. Figures 7 and 8 show the sequential images of polygonal methane hydrate crystals growing in three dimension at 276.0 K/3.70 MPa and 276.0 K/3.80 MPa, corresponding to two relatively low subcoolings 0.8 and 1.0 K, respectively. As shown by them, once a polygonal crystal appears at the front of the hydrate film in the form of a thin prism, it begins to grow in a peculiar way: (1) the basal face (bottom face) grows much faster than the top face of the crystal, as it contacts to gas phase directly, the top face nearly remains unchanged with the elapsed time; (2) the height of the crystal increases accompanying with the growth of basal face. This kind of growth way makes the crystal become a typical prismaid (see Figures 7a–d and 8a–e). As the top and bottom faces of prismaid are of different areas, the gaps among neighboring crystals emerge certainly. This kind of gaps largely favors the transfer of water molecules, increases the interface area between hydrate crystals and water phase, and, therefore, favors the further growth of hydrate crystals.[35] Another interesting phenomenon is that the crystal sends forth new crystal in its side face near bottom, when it grows to a certain scale (see Figure 7b). The growth of new crystal may hinder the growth of mother crystal (see Figures 7c,d), as the appearance of a new crystal breaks the contact of water and methane in front of the mother crystal. This behavior makes a single crystal never grow to a bulk scale and results in porous polycrystalline bulk hydrate film. The size of single crystal should be controlled by lateral growth rate of hydrate film, because only the crystals in film front have the chance to contact with both water and gas phase. At lower lateral growth rate, the crystals in film front get more time to grow to larger one. That is why higher subcooling, higher lateral growth rate, and thinner hydrate film. It should be noted that the growth of hydrate front in thickness stated above can only be observed clearly under lower subcoolings.

At very low subcoolings, the initial thickness of the hydrate front fluctuates with time because of the large differences in the size and shape of hydrate crystals in film front, the origination of new crystals, and comparable growth rate of single crystal with that of hydrate film in lateral. This leads to larger uncertainty in the film thickness measurement at subcoolings less than 1 K. That is why the experimental data measured under subcooling lower than 1.0 K deviate from the fitted line obviously in Figure 5. That is also why the surface of hydrate film formed at lower subcooling looks rougher. At higher subcoolings, the time for growth in thickness is largely shortened due to the high propagation rate of smaller crystals that the film thickness can be taken as a constant in different positions in modeling the lateral growth rate.[14,16,18] So the method used for film thickness

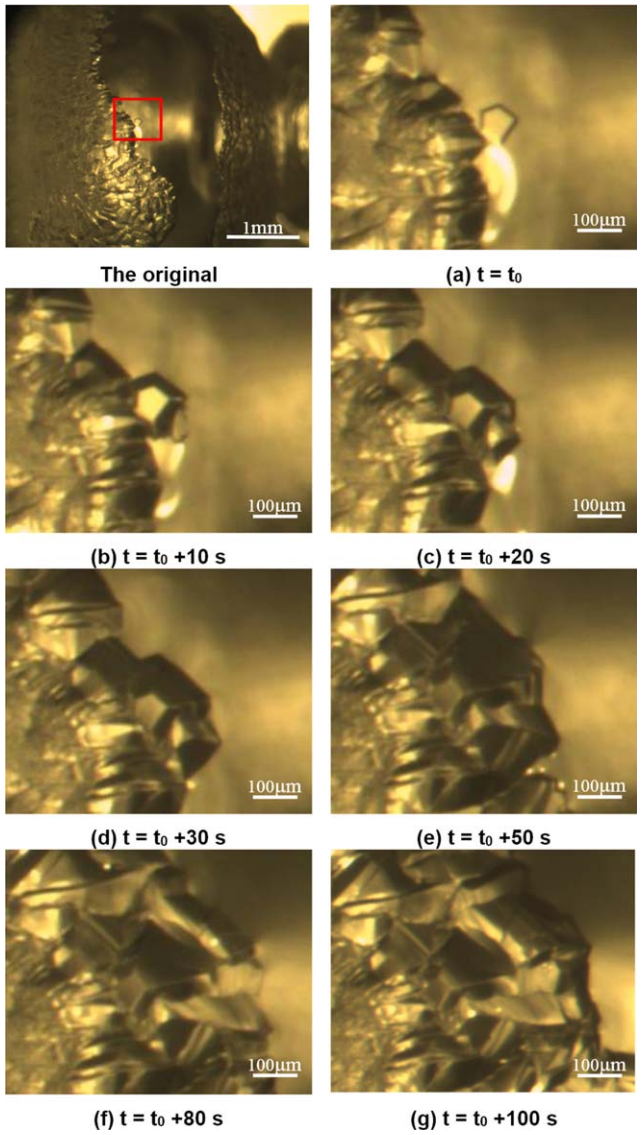

Figure 7. Sequential images of polygons growing laterally and in thickness for CH_4 + water system with the subcooling of 0.8 K when at 276.0 K.

[Color figure can be viewed in the online issue, which is available at wileyonlinelibrary.com.]

measurement in this work is more applicable to the cases of higher subcoolings, that is, $\Delta T > 1.0$ K. However, when subcooling is higher than 3 K, the hydrate film becomes so thin that its thickness is hard to be measured by a microscope.

As discussed earlier, the growth of hydrate front in Figures 7 and 8 is confined on the underneath basal face and the edge of the polygon. The growth of the hydrate crystals at the bottom basal face of polygon is mainly the hydration process of water. This is very similar to the growth of ice crystals in subcooled water.[32] Thus, the growth in thickness of hydrate film may be governed by the similar interfacial kinetics as ice crystals.[32] Theoretical analysis[37–40] and experimental measurements[41] of growth rates of ice crystals have been performed systematically. The growth rate in thickness of hydrate crystals in front of the hydrate film could be assumed expressed in the form of power law as that of the ice crystals,[41] that is

$$\upsilon_t = k_t(\Delta T)^{\alpha} \tag{2}$$

where υ_t is the growth rate in thickness of the hydrate crystals. According to the growth of ice crystals, in different subcooling regions, power α is determined by the most ubiquitous growth mechanisms of two-dimensional nucleation or spiral growth[41,42] and equals to 2 for 0.2 K $< \Delta T <$ 0.5 K and 1 for $\Delta T > 0.5$ K, respectively.[41] Then υ_t is determined at a certain subcooling in experiments, and the growth in thickness of hydrate crystals is controlled by the growth time in thickness. With the decrease of the subcooling, the time for the growth of hydrate front in thickness is prolonged by the decrease of lateral growth rate. The growth of hydrate front in thickness should become more obvious with the decreasing subcooling and predominate hydrate film growth when the subcooling is low enough. The phenomenon was also observed experimentally in the hydrate film growth at a subcooling of 0.2 K as shown in Figure 9. The hydrate film growth in thickness is observed in the whole time. The hydrate film front is markedly thick with the growth of hydrate film. It can be observed that the growth in thickness is more obvious than that in lateral at $\Delta T = 0.2$ K.

In addition, the comparison of the 3-D growth pattern of hydrates and ice can be conducive to working out the

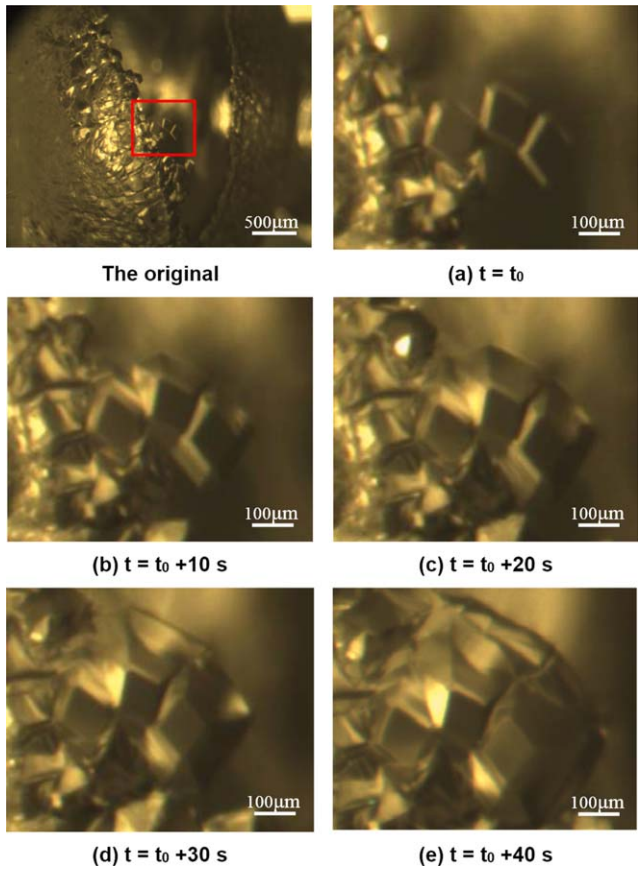

Figure 8. Sequential images of polygons growing laterally and in thickness for CH_4 + water system with the subcooling of 1.0 K when at 276.0 K.

[Color figure can be viewed in the online issue, which is available at wileyonlinelibrary.com.]

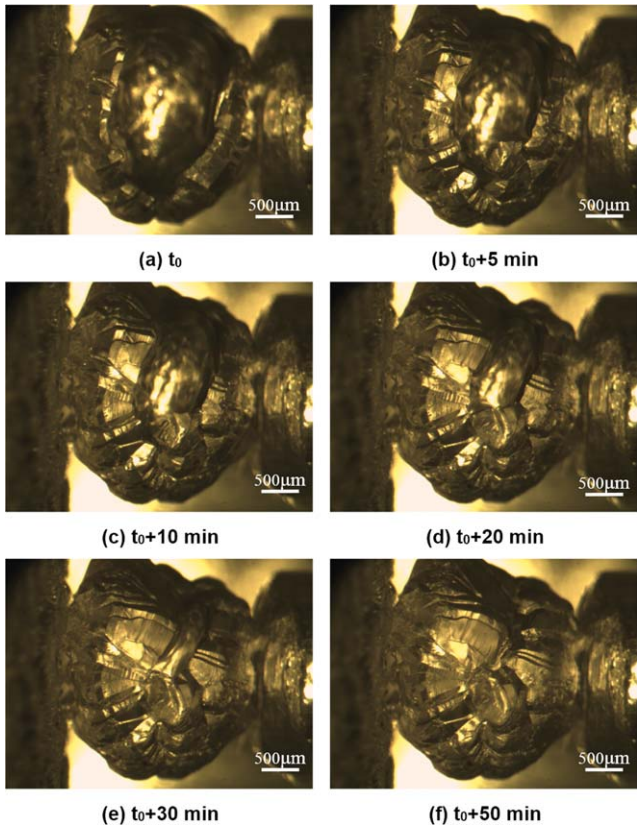

Figure 9. Methane hydrate film growing on the surface of the bubble for CH_4 + water system with the subcooling of 0.2 K when at 276.0 K.

[Color figure can be viewed in the online issue, which is available at wileyonlinelibrary.com.]

mechanism of hydrate crystal growth in other ways. The power law that was taken from the growth mechanism of the ice crystals and applied to describe the relationship between the growth rate in thickness of hydrate film and the subcooling will provide a new principle to understand the growth mechanism of the hydrate film growing in thickness. But when the hydrate shell completely covers the surface of bubble, mass transfer directly through the hydrate film dominates the growth kinetics of hydrate in thickness, and the mechanism of hydrate growth under this condition is totally different from that of the ice crystals.

Growth in thickness of hydrate shell

After the hydrate film covers on the surface of suspended bubble, the bubble is like being enclosed by a hydrate shell. The growth in thickness of hydrate shell is studied through observing its morphological change in this work. Figure 10 shows the time-dependent morphological change of methane hydrate shell formed at 274.0 K and 2.82 MPa, with a subcooling of 0.4 K. As shown in Figure 10, at t_f, the time when the hydrate shell was initially formed on the bubble surface, the surface of the shell is quite coarse. This morphology characteristic demonstrates that hydrate shell is a polycrystal with nonuniform thickness. The thickening rate at thinner positions should be higher than that at thicker position because of lower mass-transfer resistance. Thus, with the time elapsed, the thickness difference in different positions decreases, and the shell surface becomes smoother and smoother. The two shots taken at t_f and t_f + 30 min are shown in Figure 10. As the mass transfer directly through the hydrate film, the hydrate surface changes from roughness to smooth with the time elapsed, and the gaps among neighboring crystals in the film diminish. It may sink from its surface with the continuous consumption of gas inside the bubble, as shown in Figure 10b (see the area denoted by the arrows). This phenomenon appears earlier and is more significant at high subcooling as shown in Figure 11b for methane hydrate shell formed at 276.0 K and 4.10 MPa with a subcooling of 1.8 K (see the area denoted by an arrow).

Conclusions

The hydrate film growth on a single methane bubble suspended in pure water was observed by a microscope. It was found that the film front is entirely in the water phase. Based on this finding, we measured the initial thicknesses of CH_4 hydrate film at different subcoolings and three fixed temperatures of 274.0, 276.0, and 278.0 K through determining the vertical distance between the outer surface of hydrate film and that of methane bubble using a microscope and a CCD camera. The experimental results show that the initial film thickness is mainly subcooling dependent and varies with it inversely in higher subcooling region, that is, $\Delta T > 1.0$ K. At subcooling region lower than 1.0 K, initial thickness of film becomes both temperature and subcooling dependent and fluctuates with elapsed time. This is because the lateral propagating rate of hydrate crystals is very low, and single hydrate crystal at film front has sufficient time to grow to nonuniform 3-D shape, which were clearly observed and

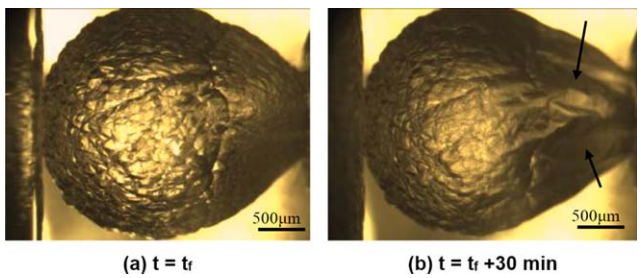

Figure 10. Changes of hydrate shell for CH_4 + water system at the subcooling of 0.4 K when at 274.0 K.

[Color figure can be viewed in the online issue, which is available at wileyonlinelibrary.com.]

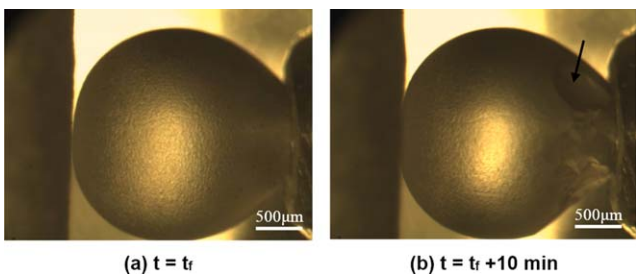

Figure 11. Changes of hydrate shell for CH_4 + water system at the subcooling of 1.8 K when at 276.0 K.

[Color figure can be viewed in the online issue, which is available at wileyonlinelibrary.com.]

recorded. At subcoolings lower enough, it was observed that the lateral growth of hydrate film was controlled by the 3-D growths of individual hydrate crystals at film front; the growth in thickness becomes more notable than in lateral. The growth mechanism of ice crystal in subcooled water was adopted to further interpret these phenomena, as we found that there existed similarity between the 3-D growth pattern of hydrate film front and ice. The experimental data of initial film thickness measured at higher subcoolings were compared with calculation results based on different film lateral growth models. It was demonstrated that Peng et al.'s[18] model gives the good evaluation to the initial thickness of methane hydrate film. The growth in thickness of hydrate shell covering one whole methane bubble surface was also investigated by observing its morphology change with elapsed time at different subcoolings. It was found that the hydrate shell surface became smoother and smoother with elapsed time because of the continuing film growth in thickness. The growth of hydrate shell in thickness may also result in the shrink phenomenon, indicating the remarkable consumption of gas inside the shell.

Acknowledgments

The financial support received from the National 973 Project of China (No. 2009CB219504), National Natural Science Foundation of China (Nos. 20925623, U1162205, and 21076225), and Science Foundation of China University of Petroleum, Beijing (No. LLYJ-2011-63) is gratefully acknowledged.

Notation

C = parameter in heat-transfer model in Ref. 18
k = inverse proportional coefficient in Eq. 1
k_t = parameter of growth rate in thickness of the hydrate crystals in Eq. 2
ΔT = the subcooling in experiments
T^{eq} = equilibrium temperature of hydrate formation at experimental pressure
T^{exp} = temperature for hydrate film growth specified in the experiment
υ_f = lateral growth rate of hydrate film
υ_t = growth rate in thickness of the hydrate crystals

Greek letters

α = exponent of subcooling in Eq. 2
δ = initial thickness of hydrate film
ψ = parameter of lateral growth rate in Ref. 18

Literature Cited

1. Boswell R. Is gas hydrate energy within reach? *Science* 2009;325:956–957.
2. Nagai Y, Yoshioka H, Ota M, Sato Y, Inomata H, Smith RL Jr, Peters CJ. Binary hydrogen–tetrahydrofuran clathrate hydrate formation kinetics and models. *AIChE J*. 2008;54:3007–3016.
3. Sugahara T, Haag JC, Prasad PSR, Warntjes AA, Sloan ED, Sum AK, Koh CA. Increasing hydrogen storage capacity using tetrahydrofuran. *J Am Chem Soc*. 2009;131:14616–14617.
4. Hu YH, Ruckenstein E. Clathrate hydrogen hydrate—a promising material for hydrogen storage. *Angew Chem Int Ed*. 2006;45:2011–2013.
5. Florusse LJ, Peters CJ, Schoonman J, Hester KC, Koh CA, Dec SF, Marsh KN, Sloan ED. Stable low-pressure hydrogen clusters stored in a binary clathrate hydrate. *Science*. 2004;306:469–471.
6. Schuth F. Technology: hydrogen and hydrates. *Nature*. 2005;434:712–713.
7. Kumar R, Linga P, Moudrakovski I, Ripmeester JA, Englezos P. Structure and kinetics of gas hydrates from methane/ethane/propane mixtures relevant to the design of natural gas hydrate storage and transport facilities. *AIChE J*. 2008;54:2132–2144.
8. Sloan ED. Fundamental principles and applications of natural gas hydrates. *Nature*. 2003;426:353–359.
9. Koh CA, Sloan ED. Natural gas hydrates: recent advances and challenges in energy and environmental applications. *AIChE J*. 2007;53:1636–1643.
10. Martínez MC, Dalmazzone D, Fürst W, Delahaye A, Fournaison L. Thermodynamic properties of THF + CO_2 hydrates in relation with refrigeration applications. *AIChE J*. 2008;54:1088–1095.
11. Lehmkühler F, Paulus M, Sternemann C, Lietz D, Venturini F, Gutt C, Tolan M. The carbon dioxide−water interface at conditions of gas hydrate formation. *J Am Chem Soc*. 2008;131:585–589.
12. Liang S, Kusalik PG. The mobility of water molecules through gas hydrates. *J Am Chem Soc*. 2011;133:1870–1876.
13. Sun CY, Chen GJ, Ma CF, Huang Q, Luo H, Li QP. The growth kinetics of hydrate film on the surface of gas bubble suspended in water or aqueous surfactant solution. *J Cryst Growth*. 2007;306:491–499.
14. Mori YH. Estimating the thickness of hydrate films from their lateral growth rates: application of a simplified heat transfer model. *J Cryst Growth*. 2001;223:206–212.
15. Mochizuki T, Mori YH. Clathrate-hydrate film growth along water/hydrate-former phase boundaries-numerical heat-transfer study. *J Cryst Growth*. 2006;290:642–652.
16. Uchida T, Ebinuma T, Kawabata Ji, Narita H. Microscopic observations of formation processes of clathrate-hydrate films at an interface between water and carbon dioxide. *J Cryst Growth*. 1999;204:348–356.
17. Freer EM, Sami Selim M, Sloan ED. Methane hydrate film growth kinetics. *Fluid Phase Equilib*. 2001;185:65–75.
18. Peng BZ, Dandekar A, Sun CY, Luo H, Ma QL, Pang WX, Chen GJ. Hydrate film growth on the surface of a gas bubble suspended in water. *J Phys Chem B*. 2007;111:12485–12493.
19. Taylor CJ, Miller KT, Koh CA, Sloan ED. Macroscopic investigation of hydrate film growth at the hydrocarbon/water interface. *Chem Eng Sci*. 2007;62:6524–6533.
20. Ohmura R, Shimada W, Uchida T, Mori YH, Takeya S, Nagao J, Minagawa H, Ebinuma T, Naritay H. Clathrate hydrate crystal growth in liquid water saturated with a hydrate-forming substance: variations in crystal morphology. *Philos Mag*. 2004;84:1–16.
21. Ohmura R, Kashiwazaki S, Mori YH. Measurements of clathrate-hydrate film thickness using laser interferometry. *J Cryst Growth*. 2000;218:372–380.
22. Makogon Y, Makogon T, Holditch S. Several aspects of the kinetics and morphology of gas hydrates. In: Proceedings of the Japan National Oil Conference, Chiba City, Japan, Oct. 20-28, 1998.
23. Servio P, Englezos P. Morphology of methane and carbon dioxide hydrates formed from water droplets. *AIChE J*. 2003;49:269–276.
24. Kobayashi I, Ito Y, Mori YH. Microscopic observations of clathrate-hydrate films formed at liquid/liquid interfaces. *I. Morphology of hydrate films*. *Chem Eng Sci*. 2001;56:4331–4338.
25. Ohmura R, Matsuda S, Uchida T, Ebinuma T, Narita H. Clathrate hydrate crystal growth in liquid water saturated with a guest substance: observations in a methane + water system. *Cryst Growth Des*. 2005;5:953–957.
26. Sugaya M, Mori YH. Behavior of clathrate hydrate formation at the boundary of liquid water and a fluorocarbon in liquid or vapor state. *Chem Eng Sci*. 1996;51:3505–3517.
27. Hirai S, Tabe Y, Kuwano K, Ogawa K, Okazaki KEN. MRI measurement of hydrate growth and an application to advanced CO2 sequestration technology. *Ann NY Acad Sci*. 2000;912:246–253.
28. Watanabe S, Saito K, Ohmura R. Crystal growth of clathrate hydrate in liquid water saturated with a simulated natural gas. *Cryst Growth Des*. 2011;11:3235–3242.
29. Ishida Y, Sakemoto R, Ohmura R. Crystal growth of clathrate hydrate in gas/liquid/liquid system: variations in crystal-growth behavior. *Chem Eur J*. 2011;17:9471–9477.
30. Tanaka R, Sakemoto R, Ohmura R. Crystal growth of clathrate hydrates formed at the interface of liquid water and gaseous methane, ethane, or propane: variations in crystal morphology. *Cryst. Growth Des*. 2009;9:2529–2536.
31. Ohmura R, Matsuda S, Itoh S, Ebinuma T, Narita H. Formation and growth of structure-H hydrate crystals on a water droplet in contact

with methane gas and a large-molecule guest substance liquid. *Cryst Growth Des*. 2005;5:1821–1824.
32. Jin Y, Nagao J. Morphological change in structure H clathrates of methane and liquid hydrocarbon at the liquid–liquid interface. *Cryst Growth Des*. 2011;11:3149–3152.
33. Sun CY, Peng BZ, Dandekar A, Ma QL, Chen GJ. Studies on hydrate film growth. *Annu Rep Prog Chem Sect C: Phys Chem*. 2010;106:77–100.
34. Chen GJ, Guo TM. Thermodynamic modeling of hydrate formation based on new concepts. *Fluid Phase Equilib*. 1996;122:43–65.
35. Kuhs WF, Genov GY, Goreshnik E, Zeller A, Techmer K, Bohrmann G. The impact of porous microstructures of gas hydrates on their macroscopic properties. *Int J Offshore Polar Eng*. 2004;14: 305–309.
36. Kirchner MT, Boese R, Billups WE, Norman LR. Gas hydrate single-crystal structure analyses. *J Am Chem Soc*. 2004;126:9407–9412.
37. Shimada W, Furukawa Y. Pattern formation of ice crystals during free growth in supercooled water. *J Phys Chem B*. 1997;101:6171–6173.
38. Nada H, Furukawa Y. Anisotropy in molecular-scaled growth kinetics at ice−water interfaces. *J Phys Chem B*. 1997;101:6163–6166.
39. Yokoyama E, Sekerka RF, Furukawa Y. Growth of an ice disk: dependence of critical thickness for disk instability on supercooling of water. *J Phys Chem B*. 2009;113:4733–4738.
40. Yokoyama E, Sekerka RF, Furukawa Y. Growth trajectories of disk crystals of ice growing from supercooled water. *J Phys Chem B*. 1999;104:65–67.
41. Yokoyama E, Yoshizaki I, Shimaoka T, Sone T, Kiyota T, Furukawa Y. Measurements of growth rates of an ice crystal from supercooled heavy water under microgravity conditions: basal face growth rate and tip velocity of a dendrite. *J Phys Chem B*. 2011;115:8739–8745.
42. Sazaki G, Zepeda S, Nakatsubo S, Yokoyama E, Furukawa Y. Elementary steps at the surface of ice crystals visualized by advanced optical microscopy. *Proc Natl Acad Sci USA*. 2010;107:19702–19707.

Manuscript received Mar. 13, 2012, and revision received Nov. 12, 2012.